PERFORMANCE ANALYSIS OF SOLAR ASSISTED MULTIGENERATIONAL SYSTEM USING THERMINOL VP1 BASED NANOFLUIDS: A COMPARATIVE STUDY

***Muhammad S. KHAN*[1], *Khuram P. AMBER*[1], *Hafiz M. ALI*[*2], *Muhammad ABID*[3], *Tahir A. H. RATLAMWALA*[4], *Samina JAVED*[2]**

[1]Department of Mechanical Engineering, Mirpur University of Science and Technology (MUST), Mirpur-10250 (AJK), Pakistan

[*2]Department of Mechanical Engineering, University of Engineering and Technology, Taxila 47050, Pakistan

[3]Department of Energy Systems Engineering, Faculty of Engineering, Cyprus International University, Northern Cyprus, Turkey.

[4]Department of Engineering Sciences, National University of Science and Technology (NUST), Karachi, Pakistan

* Corresponding author; E-mail: h.m.ali@uettaxila.edu.pk

The application of the nanofluids is suggested to enhance and improve the efficiency of solar thermal power system. In the present study, three different nanofluids (Fe_2O_3/therminol VP1, SiO_2/therminol VP1 and Cu/therminol VP1) are numerically investigated in parabolic dish solar collector that is further integrated to a combined cycle for power and hydrogen production. Heat rejects from the power cycle is also utilized to drive a single effect absorption (LiBr/water) system. Furthermore, a comprehensive energy, exergy and exergo-environmental analysis are carried out by varying several input parameters and their influence on overall energetic and exergetic efficiencies, network output and rate of hydrogen generation is assessed. The engineering equation solver (EES) is employed to conduct the parametric study. Outcomes of the study demonstrate that the SiO_2/VP1 has the better characteristics among the investigated nanofluids. The overall energetic efficiency of the SiO_2/VP1, Fe_2O_3/VP1 and Cu/VP1 is almost 38.79%, 38.74% and 37.53%, while overall exergetic efficiency is 41.72%, 41.66% and 40.36%, respectively at 1000 Wm^{-2}. The exergoenvironmental impact coefficient and impact index are noticed to be reduced for all the three nanofluids as mass flow rate increases. The hydrogen production rate for SiO_2/VP1 is maximum and has observed to be increased by increasing the ambient temperature. Increase in nanoparticles concentration also rises the exergetic efficiency but reduces the thermal conductivity of the nanofluids. Coefficient of performance is noticed to be increased with rise in evaporator temperature, whereas, it is reduced by increasing the generator temperature.

Keywords: *Parabolic dish, Exergo-environmental, Hydrogen, Nanofluids*

1. Introduction

The application of renewable energy resources (especially solar) is the best solution to tackle the environmental threats (CO, CO_2 emissions, depletion of Ozone, etc.) that are due to the burning of conventional energy fuels. Therefore, energy demand for the society through sustainable and clean recourses is the prime and the most important challenge [1]. The concentrated solar power systems are used for high temperature applications and parabolic dish collector has the highest solar to thermal conversion efficiency [2]. Le Roux et al. [3] proposed a rectangular cavity dish receiver model applied as a heat source for Brayton cycle. An experimental and numerical study on the cavity receiver of dish collector was performed by Qiu et al. [4]. Although, there are various working fluids (molten salts, synthetic oil) that can be used as a heat transfer fluid (HTF) in the collector loop. However, such fluids are not suitable due to their flammability and toxicity. Under such circumstances, nanofluids are more suitable HTF option for the solar collectors. He et al. [5] experimentally investigated the performance of a vacuum tube solar receiver using carbon nanotube/water and TiO_2/water. The Al_2O_3/ Therminol VP1 nanofluid was examined in a concentrated parabolic solar collector by Khullar et al.[6] and a comparison between experimental results of a conventional parabolic concentrating solar collector was presented. Nanoparticles of four various sizes with different volume concentrations were investigated in a flat plate collector by Mahian et al. [7]. Sajid and Ali [8] studied the application of nanofluids in various heat transfer devices such as, heat sinks, shell and tube heat exchangers and plate type heat exchangers. Different experimental and numerical validated correlations have been assessed and compared. A numerical model of parabolic dish solar collector using two different nanofluids was developed and investigated from thermal and exergetic point of views [9]. The performance of PV/thermal solar collector was analysed by considering influence of lower and upper reflector and water based nanofluid [10]. They concluded that outlet temperature of water increased by 0.44% using nanofluid as a cooling medium. Laaraba [11] studied numerically the performance of flat plate solar thermal collector by adding partitions to the glazing wall. It was found that this addition reduced the thermal losses to the surroundings because of the decrease in Nusselt number. Daily performance of solar dish collector under different inlet temperature levels was studied by Pavlovic etal. [12]. Collector thermal efficiency decreased between 67.36% and 54.65% with rise in temperature from 823 K to 523 K. In contrast to individual Brayton or Rankine cycle, the combined cycles have received great attention because of their higher thermal efficiency in the design of power plants. The integration of combined gas cycle with solar energy is a cheaper way to harness solar thermal power [13], even at low solar input. Spelling et al. [14] conducted a thermo-economic optimization of combined power plant integrated with solar system. A detailed second law efficiency investigation of combined cycle (ORC) integrated to a parabolic trough solar collector using seven different refrigerants was performed by Al-Sulaimen [15]. The exergy analysis of solar systems was conducted by Dincer and Rosen [16]. A tri-generation ORC was investigated from exergoenvironmental point of view by Ahmadi et al. [17], while a small scale integrated hydrogen and power generation system was exergo-economically analyzed by Caliskan et al. [18]. Parham et al. [19] accomplished a comprehensive thermodynamic and environmental analysis of a multi-production system having ORC, internal heat exchanger, open absorption heat transformation and an electrolyser. Hydrogen can be used as a fuel and offers exceptional advantages helping hydrogen to become one of the most important energy carrier in the future [20]. Electric power can be generated by the utilization of hydrogen in fuel cells. Researchers [21-22] explored hydrogen for the purpose of friendly ecology and clean fuel. Various solar integrated hydrogen generation systems were examined by the researchers [23-24]. The most effective method to produce hydrogen on commercial scale is the water electrolysis [25]. The absorption refrigeration cycles are environmentally friendly as they use non-chlorofluorocarbons and usually working on low temperatures. These cycles mostly work on ammonia/water and lithium bromide/water as working pairs [26]. Bahman [27] studied comprehensively a single effect aqueous Li-Br vapor absorption system that was driven by a Flat plate solar collectors. The small absorption systems (LiBr/water) were observed for their cooling capacities and COP by Asdrubali et al. [28]. Different operating conditions were associated to the COP of the absorption system. Similarly, Vega et al. [29] investigated the performance of a single effect (SE) absorption cycle experimentally. From the literature, it is evident that the detailed energy, exergy and exergo-environmental analysis of dish solar collector integrated to a combined cycle for power, cooling and hydrogen production is very rare. The researchers focused only on the energy and exergy analysis of integrated parabolic trough collectors and heliostat field with combine power cycles for electricity and heating/cooling purposes. To fill this gap, the current study aims to investigate the comprehensive energy, exergy and exergo-environmental analysis of parabolic dish solar collector integrated with combined cycle using three different nanofluids (Fe_2O_3/therminol VP1, SiO_2/therminol VP1 and Cu/therminol VP1). The useful heat gain from the collector is utilized to drive the combined cycle to generate electricity, while some portion of the turbine work output is fed to the electrolyser for rate of hydrogen production. Moreover, a SE absorption Li-Br/ water system is also powered by the waste heat of power cycle to produce hydrogen.

2. System description

The proposed system as shown in Figure 1 includes a PDSC (cavity receiver), integrated with combine power plant, an electrolyser and a single effect absorption cycle for electricity, hydrogen production and cooling. The heat gained by the absorber tube of PDSC depicted in Figure 2, is transferred to the HTFs and then as a useful heat to the heat exchanger "**A**" of the Brayton cycle. In a CCPP, work is done in two stages, air is working fluid in Brayton cycle and water is used in steam cycle. In heat exchanger "**A**", heat of the nanofluids from collector is transferred to the air circulating in the gas cycle. The gas compressor between states points 32 and 33 compresses this air to increase its pressure and temperature and then enters to the gas turbine at point 3 for useful work. The pressure of the hot air is decreased by passing through the gas turbine and it enters to the heat exchanger 1 of the steam cycle. The temperature of the hot air at point 4 is high enough to further heat the working fluid of the steam cycle. This high pressure high temperature steam is used to drive the high pressure steam, generating power output and steam expands at point 6 and after again reheating, moves to the steam turbine 2 for producing electricity. The maximum portion of power from turbine is used for buildings at state point 30, whereas, small part is fed into the electrolyzer at point 31 for hydrogen production. The steam becomes saturated liquid by passing through condenser between state points 8 and 9, while pump 1 between state points 9 and 10 pumps the saturated liquid back towards the steam turbine 1 for recycling.

The air leaving the heat exchanger at state 11 has relatively high temperature to power a single effect absorption chiller. The lithium bromide/ water mixture is used in absorption cycle. At states 15, 16 and 17 solution is a weak, while, at states 12, 13 and 14 it is strong. The weak solution at point 15 is compressed by the pump and after heating via heat exchanger 2, it enters to the generator. The solution gets heated in the generator and splitting out the water vapors. The vapors at state 18 go to the condenser, rejecting heat and then proceed to the refrigerant valve at point 19 as a saturated liquid. It becomes saturated liquid vapor mixture t state 20 after passing through the refrigerant valve and then this mixture enters into the evaporator, exchanging heat to the surroundings producing cooling effect and enters the absorber. The strong solution at state 12 comes to the heat exchanger by giving heat to the weak solution and enters to the solution valve at 13 and finally to the absorber where it absorbs the low grade vapor and reduces its temperature by discarding heat to the environment.

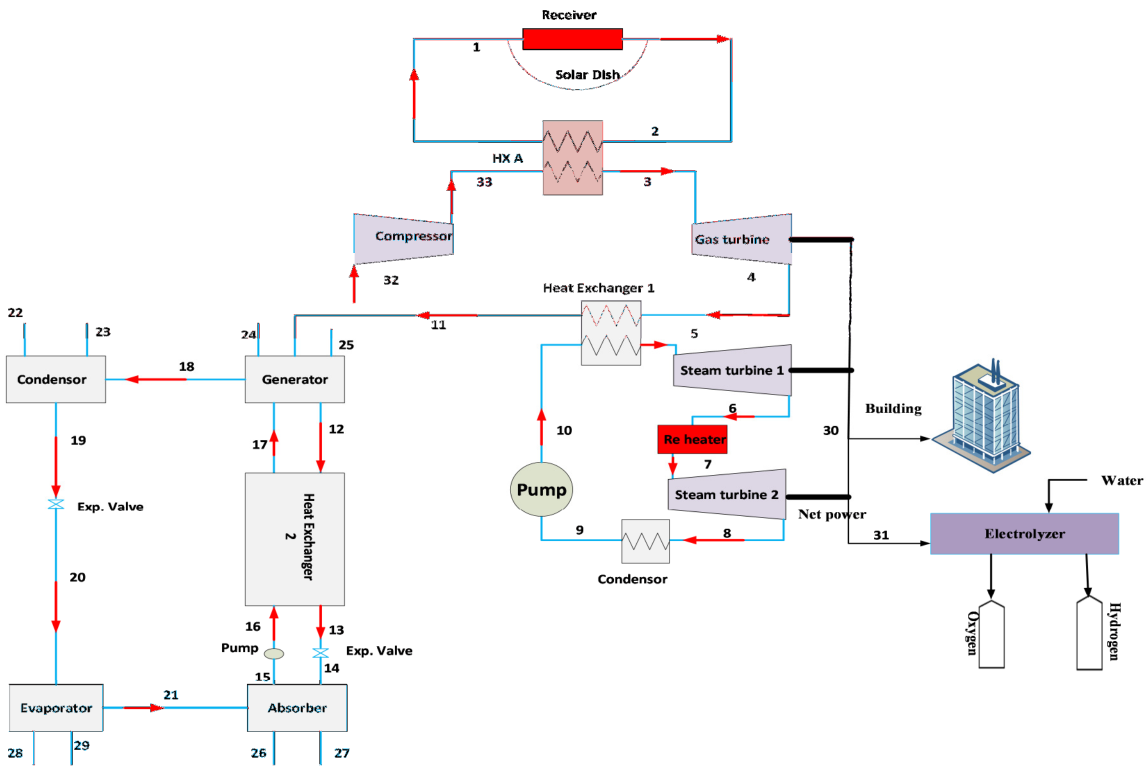

Fig. 1. Proposed solar assisted multigenerational system

3. Methodology

This section presents the methodology to solve the mathematical models of the solar integrated multigenerational system. The integrated system consists of the parabolic dish collector with nanofluids as a heat transfer fluid, combined gas cycle, single effect lithium bromide absorption cycle chiller and hydrogen production system. The parametric analysis are conducted using engineering equation solver (EES). Assumptions consider for the solar integrated multigenerational system are, pressure drop in pipes and heat exchanger is negligible with zero heat transfer to the surroundings. Steady state conditions are considered. Ambient temperature is 300 K, while receiver inlet temperature is 350 K. The design parameters for Single Effect Absorption System, combined cycle and PDSC are given Tables 1, 2 and 3 respectively.

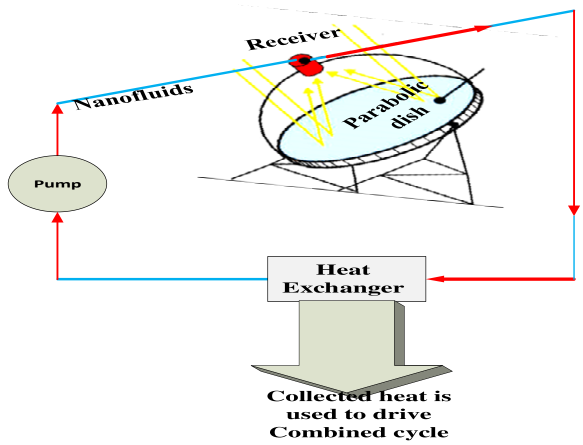

Fig. 2. Solar dish collector with receiver

Table 1: Design parameters for S.E absorption system [26]

Parameter	**Value**
Capacity	1,001 (kW)
Evaporator Temperature	282 (K)
Exit Temperature of Generator Solution	342 (K)
Exit Temperature of Generator Vapor	338.8 (K)
Solution Heat Exchanger Exit Temp.	334.8 (K)
Heat Exchanger Effectiveness	70 (%)
Pump Efficiency	100 (%)

Table 2: Input parameters for combined cycle [34, 38]

ambient temperature	300 K
ambient pressure	100 kPa
isentropic efficiency of compressor	80%
isentropic efficiency of pump	80%
isentropic efficiency of gas turbine	80%
steam turbine isentropic efficiency	80%
first steam turbine inlet pressure	6000 k Pa [38]
compressor outlet pressure	700 kPa
condenser inlet pressure	10 kPa
second steam turbine inlet pressure	1000 kPa [38]
gas turbine exit temperature	100 kPa
second steam turbine inlet Temperature	741K

Table 3: Input data used for PDSC [20, 33]

optical efficiency	η_o	85% [20]
thermal conductivity	k	15 $W.m^{-1}K$
emissivity of receiver	ε_r	90%
mass flow rate	$\dot{m}$	0.06 $kg.s^{-1}$
solar radiation	G_b	1000$W.m^{-2}$
inlet temperature	T_{in}	350 K
receiver temperature	T_r	540 K
wind speed	V_{air}	1$m.s^{-1}$
receiver outer diameter	D_{ro}	0.15m
receiver inner diameter	D_{ri}	0.015m
dish radius	R	2m

length of receiver	L	15m
temperature of the sun	T_s	5700K [33]

3.1 Nanofluids properties

The nanofluids considered in the present study are Fe_2O_3/therminol VP1, SiO_2/therminol VP1 and Cu/therminol VP. The thermophysical properties of the nanofluids are higher in comparison to base fluids therefore, they have maximum rate of heat transfer. The properties of the nanofluids are taken from [1, 20] and are presented Table 4. A higher concentration is needed for the specification of nanofluid properties to achieve correct results of the simulation model. Nanoparticles concentration ratio, temperature and thermophysical properties of base fluid highly effect the thermophysical properties of nanofluids.

Table 4. Different properties of nano particles [1, 20]

Property	Cu	SiO_2	Fe_2O_3
Thermal conductivity ($W.m^{-1}$ K)	400	1.4	5.38
Specific heat capacity ($J.kg^{-1}$ K)	385	745	726.9
Density (kgm^{-3})	8933	2220	5240

The volumetric fraction of nanoparticles is 2% to form nanofluids. The specific heat capacity and density of the nanofluids can be determined as suggested by [30, 31].

$$\rho_{nf} = \rho_{bf}.(1-\varphi) + \rho_{np}.\varphi \quad (1)$$

$$C_{p,nf} = \frac{\rho_{bf}.(1-\varphi)}{\rho_{nf}}.C_{p,bf} + \frac{\rho_{np}.\varphi}{\rho_{np}}.C_{p,np} \quad (2)$$

The viscosity, thermal diffusivity and thermal conductivity of the nanofluids can be calculated using equations as given by [32, 26].

$$\mu_{nf} = \mu_{bf} \cdot (1 + 2.5 \cdot \varphi + 6.5 \cdot \varphi^2) \quad (3)$$

$$\alpha_{nf} = \frac{k_{nf}}{(\rho C_p)_{nf}} \quad (4)$$

$$k_{nf} = \frac{k_{np} + 2.k_{bf} - 2.\varphi.(k_{bf} - k_{np})}{\frac{k_{np}}{k_{bf}} + 2 + \frac{k_{bf} - k_{np}}{k_{bf}} \cdot \varphi} \quad (5)$$

3.2 Parabolic dish solar collector (PDSC)

The concentrated solar power technology used in this study is parabolic dish system and the receiver model is taken from [33].

Energy efficiency of the dish receiver and useful energy can be calculated as:

$$\eta_{en,PDSC} = Q_u/Q_{sun} \quad (6)$$

$$Q_u = Q_r - Q_l \quad (7)$$

$$Q_l = U_L A_r (T_r - T_0) \quad (8)$$

Q_r is the solar beam radiation falling on the collector, while Q_l is the heat loss from the receiver.

The useful heat gain can be found as:

$$Q_u = \dot{m} C_p (T_{out} - T_{in}) \quad (9)$$

Amount of useful heat can also be found as:

$$Q_u = F_r A_r [(S - \frac{A_r}{A_a}) U_L (T_{in} - T_a)] \quad (10)$$

The available solar energy is the combination of beam intensity and aperture area.

$$Q_{sun} = G_b A_a \quad (11)$$

3.3 Exergy analysis

The maximum possible work potential that is produced by PD collector is found by conducting exergy analysis. The exergy efficiency can be derived by using exergy balance of a solar receiver, that is:

$$\sum \dot{E}_{x,in} - \sum \dot{E}_{x,out} - \sum \dot{E}_{x,loss} - \sum \dot{E}_{x,change} - \sum \dot{E}_{x,des} = 0 \quad (12)$$

Overall energy and exergy efficiencies of integrated system can be find as follow:

$$\eta_{en,ov} = \dot{W}_{net} / \dot{Q}_{solar} \quad (13)$$

Where $\dot{Q}_{solar}$ can be found from [31].

$$\eta_{Ex,ov} = \frac{\dot{W}_{net}}{\dot{E}_{x,solar}} \quad (14)$$

Petela model is used to find out solar exergy.

$$\dot{E}_{x,solar} = G_b A_a \eta_{pet} \quad (15)$$

$$\eta_{pet} = \left[1 - \frac{4T_0}{3T_{sun}} + \frac{1}{3}\left(\frac{T_0}{T_{sun}}\right)^4\right] \quad (16)$$

The equations used to model the combined power cycle analysis and single effect absorption system are taken from the references [34] and [35], respectively and due to the space limitations cannot be presented here.

3.4 Electrolyzer and exergo-environmental analysis

The mathematical modelling of electrolyser is important to assess the rate of hydrogen produced through electrolysis process and equations that are used to investigate the electrolyzer have adopted from [20]. Moreover, environmental analysis has received a great attention in a past few years as it determines whether Exergo-environmental assessment has based on the rate of total exergy destruction, exergetic efficiency and exergy input and output [22]. The major exergo-environmental parameters are taken from [19, 36] and will be discussed in results and discussion section only because of the space limitations.

Table 5. Validation with reference [33]

Material	η_{en} [%] PDSC
Lloyd C. Ngo	68.42
$Fe2O_3$/Therminol VP1	71.23
SiO_2/Therminol VP1	70.22
Cu/Therminol VP1	68.3

Table 6.Thermodynamic properties of the SEAS (a) present model, (b) reference [26] for SEAS.

State point	P (kPa)		T (K)		$h (kJkg^{-1})$		$s (KJ.kg^{-1}.K)$		x (% LiBr)	
	a	**b**	**a**	**b**	**a**	**b**	**a**	**b**	**a**	**b**
12	4.82	4.81	343	344	163.2	164.8	0.42	0.43	0.5694	0.5694
13	4.82	4.81	316.3	317.1	89.76	89.76	0.2548	0.26	0.5694	0.5694
14	1	1	313.7	313.5	89.76	89.76	0.2381	0.24	0.5694	0.5694
15	1	1	304.8	305	69.26	69.96	0.2079	0.21	0.5225	0.5225
16	4.82	4.81	304.8	305	69.26	69.96	0.2093	0.21	0.5225	0.5225
17	4.82	4.81	334.8	337.4	132.8	138.9	0.4069	0.43	0.5225	0.5225
18	4.82	4.81	338.8	341.3	2624	2627	8.602	8.62	0	0
19	4.82	4.81	305.4	305.4	135.1	134.8	0.4673	0.47	0	0
20	1	1	280.2	280	135.1	134.8	0.483	0.48	0	0
21	1	1	280.2	280	2513	2514	8.97	8.97	0	0

4. Results and discussion

The present section of the work gives the results in detail obtained by simulation of the solar integrated multigenerational system. The results are authenticated with the previous studies and presented in Tables 5 & 6. For parabolic dish system, energy efficiency of the receiver is almost near to the value given by Lloyd C. Ngo [33], whereas, single effect absorption system is validated with the reference [26]. The mass flow rate of the working fluid in the solar receiver is a vital parameter, which effects the efficiency of solar thermal power plants. The Fig 3 is the graphical representation of the influence of mass flow rate of three different nanofluids and their impact on the overall exergy and energy efficiencies of the integrated system. The SiO_2/Therminol VP1 has the highest values of integrated energy and exergy efficiencies, increases from 32.13% to 39.03% and 34.56% to 41.98%, respectively. The Cu/ Therminol VP 1 has the lowest efficiency values amongst the investigated nanofluids, varying from 28.08% to 37.93% for overall energy efficiency, whereas, between 30.2% and 40.79% for overall exergy efficiency. Exergoenvironmental impact coefficient (C_{ei}) and impact index (Θ_{ei}) of the three nanofluids are assessed for different values of mass flow rates. Higher values of above said performance parameters are obtained at lower mass flow rates as shown in Fig 4. There is a rapid decrease in the values of (C_{ei}) and (Θ_{ei}) between mass flow rates of 0.1 and 0.3 kgs-1 ec and after 0.3 to 0.7 a less variation has been noticed. The (C_{ei}) exergoenvironmental impact coefficient is associated with the exergetic efficiency and C_{ei} increases when exergetic efficiency will reduce. The decrease in the Cei values in present system contributes to rise the exergy efficiency which is much needed and better for environmental point of view. Exergoenvironmental impact index (Θ_{ei}) is basically the product of exergoenvironmental impact coefficient and impact factor. Exergoenvironmental impact index (Θ_{ei}) tells about the system under study, is whether or not damages the surroundings. Its value should be low for safer environment and in our study the Θ_{ei} of solar thermal system working on three different nanofluids is reducing that reflects that the system under consideration is quite safer for the environment. The overall performance of the integrated system working on three different nanofluids has been examined at various ambient temperatures. At higher ambient temperatures, the system exhibits better productivity because the heat production rate and network output will be maximum at higher ambient conditions. The SiO_2/VP1 has the maximum overall first and second law efficiencies, 38.79% and 41.72%, accordingly among the other nanofluids at ambient temperature of 300 K as seen in Fig. 5. Fig. 6 represents the influence of change in the ambient temperature on work output and hydrogen production rate of integrated system. The maximum net power production (almost 80%) is fed in to the grid for power, whereas, only 20% is used by the electrolyser for hydrogen production. According to the Table 6, the specific heat capacity of SiO_2 is greater (almost 745 $J.kg^{-1}$ K), therefore, this nanofluid is capable to produce maximum workout put as compared to the other two nanofluids.

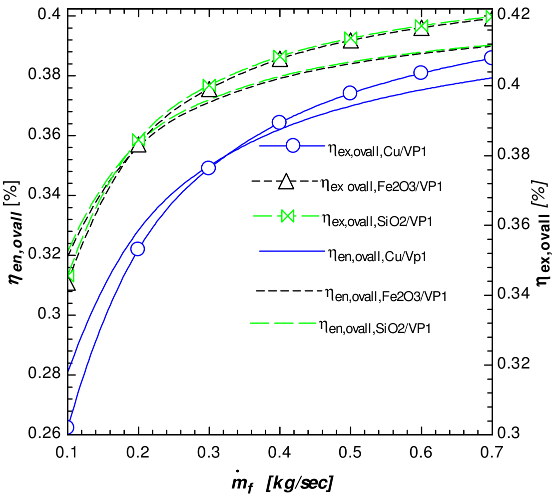

Fig. 3. Mass flow rate impact on integrated system efficiencies

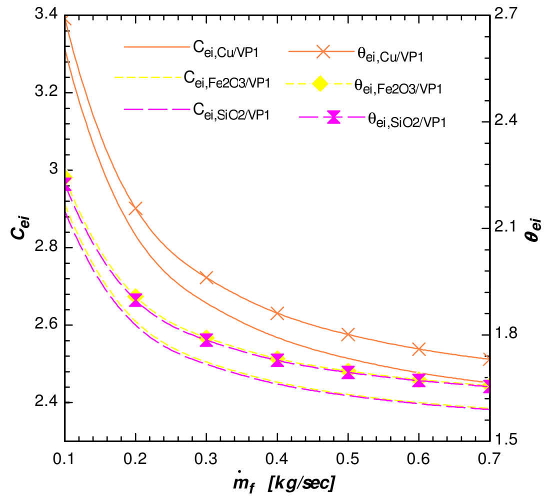

Fig. 4. Comparison of C_{ei} and θ_{ei}

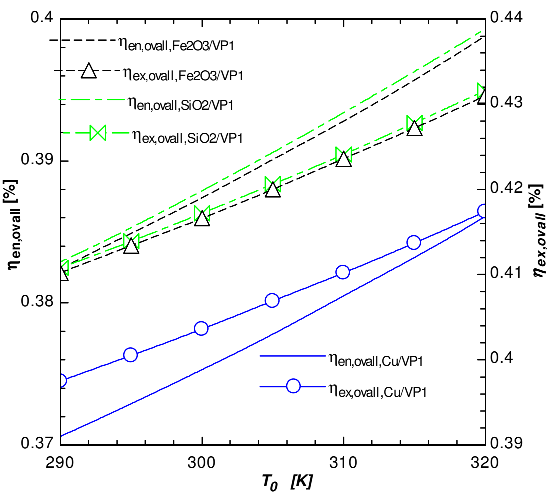

Fig 5. Comparison of integrated system efficiencies

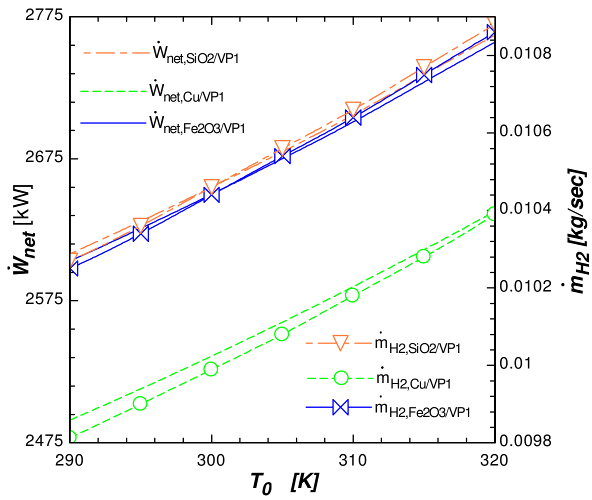

Fig 6: Comparison of net power and hydrogen production rate

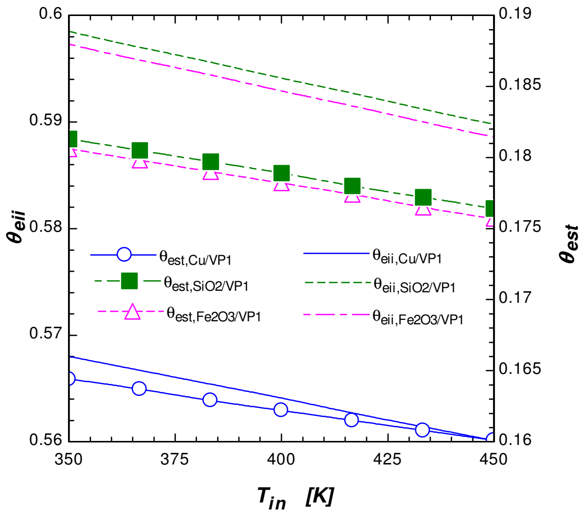

Fig 7. Inlet temperature effect on θ_{eii} and θ_{est}

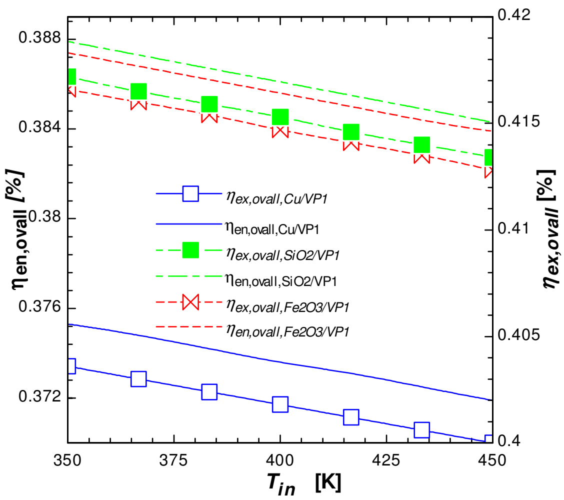

Fig 8. Inlet temperature influence on integrated system efficiencies

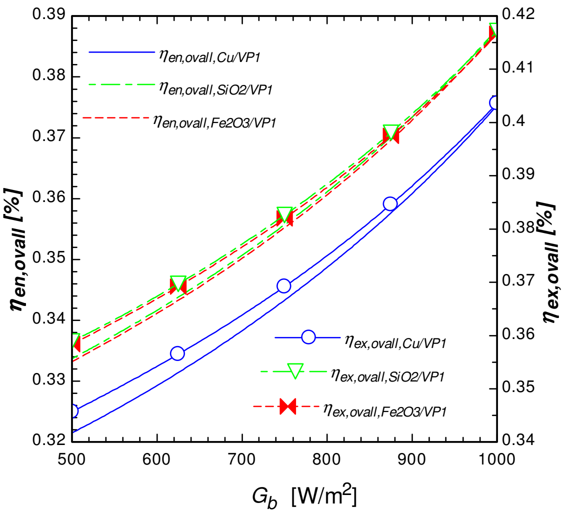

Fig 9. Solar irradiation impact on integrated system efficiencies

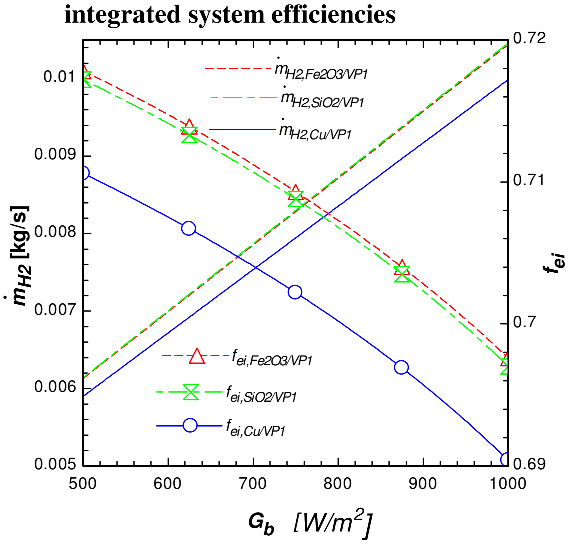

Fig 10. Effect of solar irradiation on f_{ei} and $\dot{m}_{H2}$

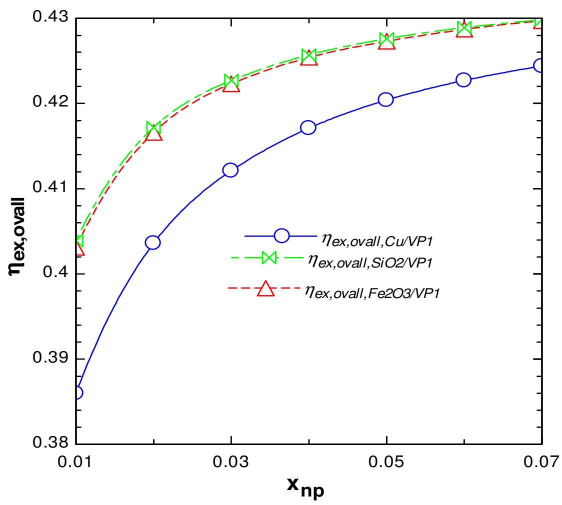

Fig 11. Comparison of integrated system exergy efficiency

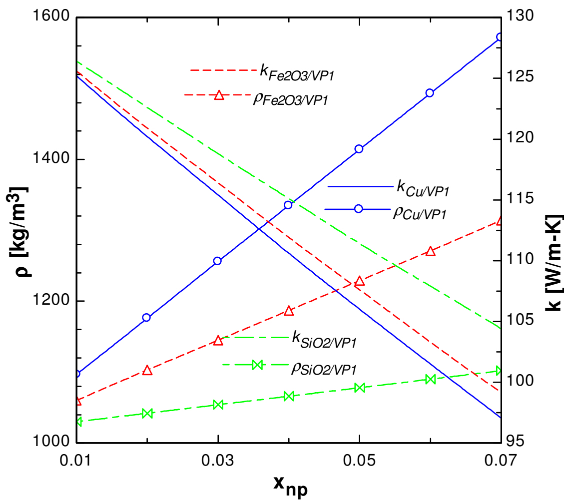

Fig 12. Variations in density & conductivity against %age concentration of nanofluids

The influence of the inlet temperature of HTF in solar receiver is plotted against exergo-environmental impact improvement (θ_{eii}) and Exergetic sustainability index (θ_{est}) as given by Fig 7. The greater value of inlet temperature of HTF causes the surface temperature of collector to be rise that ultimately increases the rate of exergy destruction. Because of this reason, useful heat as well as workout put decreases. Therefore, the maximum value of (θ_{eii}) and (θ_{est}) is obtained at lower inlet temperature (350 K). The integrated system efficiencies versus the inlet temperature are also plotted in Fig 8. The overall energy and exergy efficiencies of three nanofluids are varied from 38.79% and 38.43%, 41.72% to 41.34% for SiO_2/VP1, 38.74% to 38.43% and 41.66 to 41.28% for Fe_2O_3/VP1and 37.53% to 37.19% and 40.36% to 40% for Cu/VP1, respectively. The influence of variation in DNI from 500 to1000Wm^2 on integrated system efficiencies at constant ambient temperature and mass flow rate is plotted in Figure 9.

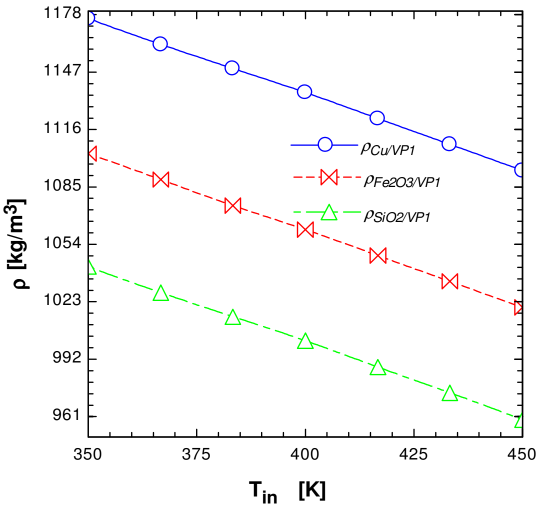

Fig 13. Variations in the densities of the nanofluids

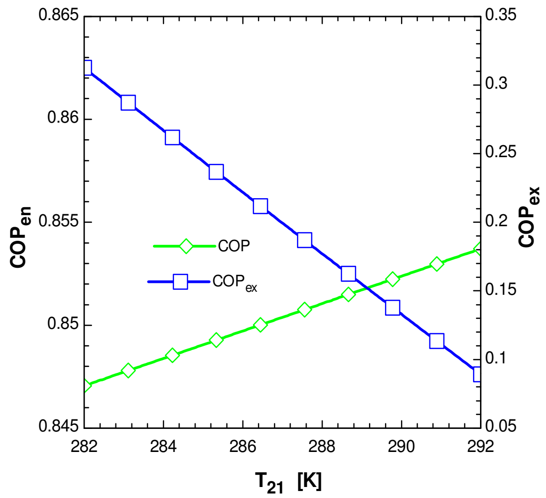

Fig 14. Evaporator temperature effect

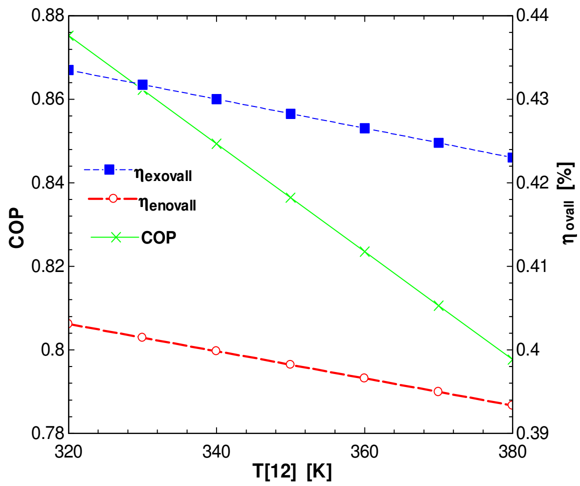

Fig 15. Generator temperature influence

Solar radiations play an important role in the performance of integrated solar thermal power plants as areas have higher solar irradiations are feasible for the installation of power plants. Higher solar irradiation intensity falling on the collector gives maximum amount of heat carried by the HTF circulating in the collector loop that ultimately contributes the higher outlet temperature [20]. Finally, network output is enhanced. The increase in the energetic and exergetic efficiencies for SiO_2/VP1 is almost linear, from 33.37 to 38.79% and 35.89% to 41.72%, respectively.

The amount of net work out is directly related with increase in the solar intensity and hydrogen production rate depends upon power output. Therefore, maximum heat production rate gives higher work output and hydrogen as well. The Figure 10 shows the influence of increase in solar radiations on the rate of hydrogen production and exergo-environmental impact factor (f_{ei}). The hydrogen production rates for three therminol-VP1 based nanofluids are increased linearly with the solar intensity. However, exergo-environmental impact factor is noticed to be reduced as DNI increases.

The total rate of exergy destruction decreases at higher values of DNI that further helps to decrease the exergo-environmental impact factor and it is very helpful to enhance the system's performance [36]. According to the environmental point of view, f_{ei} value approaching to zero is better for the environment and in present study, values of f_{ei} for all the three nanofluids are gradually moving towards the zero. Figure 11 depicts the effect of rise in the concentration of nano particles on overall exergy efficiency of the integrated solar thermal system. It can be observed that the efficiency enhances significantly by adding nano particles concentrations. The SiO_2/VP1 and Cu/VP1 have the highest and the lowest values, respectively amongst the examined fluids.

The thermal conductivity of the nanofluids is observed to be decreased while density is going to be enhanced by adding the nano particles concentration as plotted in Fig 12. The variations in the density of nanofluids is also plotted against inlet temperature of the fluid, as seen in Figure 13.

According to the environmental point of view, f_{ei} value approaching to zero is better for the environment and in present study, values of f_{ei} for all the three nanofluids are gradually moving towards the zero. Figure 11 depicts the effect of rise in the concentration of nano particles on overall exergy efficiency of the integrated solar thermal system. It can be observed that the efficiency enhances significantly by adding nano particles concentrations. The SiO_2/VP1 and Cu/VP1 have the highest and the lowest values, respectively amongst the examined fluids. The thermal conductivity of the nanofluids is observed to be decreased while density is going to be enhanced by adding the nano particles concentration as plotted in Fig 12. The variations in the density of nanofluids is also plotted against inlet temperature of the fluid, as seen in Figure 13. The performance parameter of the three nanofluids is reduced when inlet temperature increases with Cu/VP1 has the highest density among the investigated nanofluids.

The impact of rise in the evaporator temperature on the energetic as well as exergetic COPs is presented in Fig 14. COP_{en} has increased, whereas, COP_{ex} moves in an opposite way as the evaporator temperature rises. The greater value of COP is obtained at higher evaporator and less generator temperatures but the trend of COP_{ex} is in an opposite way [30]. The influence of rise in the generator temperature between 320 K and 380 K reduces the COP from 0.875 to 0.797 as well as overall energy and exergy efficiencies from 40.31% to 39.34% and 43.35% to 42.3%, respectively at T_{cond}=305.4 K and T_{evp}=281 K and is shown in Fig 15. The reason behind is that increase in the T_{gen} also boosts the strong solution concentration by maximizing the flow ratio. This phenomenon causes the reduction of the absorption heat capacity. At the end, system integrated efficiencies and coefficient of performance are reduced [37].

5. Conclusions

The current study evaluates and compares the performance of parabolic dish solar assisted multigenerational system using three different nanofluids. The multigenerational system includes combined power cycle for electricity, an electrolyser for hydrogen production and SEAS (LiBr/water) to produce cooling effect. Furthermore, exergoenvironmental analyses are also conducted in details to assess the effect of exergy losses from the integrated system. The core findings of the study are concluded here. The integrated system energy efficiency of SiO_2 based nanofluid is 38.79% and witnessed to be the higher 0.12% as compared to the Fe_2O_3 and 3.35% to Cu based nanofluids at 300 K and 1000 Wm^{-2}. Increase in mass rate of HTFs from 0.1 to 0.3 kgs^{-1} results in substantial enhancement of integrated efficiencies, 24.60% for Cu/VP1, 16.15% for Fe_2O_3/VP1 and 15.7% for SiO_2/VP1 based nanofluids. However, from 0.3 to 0.7 kgs^{-1} , less increment is found in efficiency values, 8.40%, 5.06% and 4.9%, respectively for three mentioned oil based nanofluids. Densities of Cu/VP1, Fe_2O_3/VP1 and SiO_2/VP1 are increased to almost 43%, 23% and 7%, respectively with rise in nanoparticles concentration. Furthermore, rise in the inlet temperature of the working fluid in collector reduces the density for SiO_2/VP1, Fe_2O_3/VP1 and Cu/VP1 from 1042 to 959 kgm^{-3},1103 to 1020 kgm^{-3} and 1176 to 1094 kgm^{-3}, respectively, because of the rise in the exergy losses from the receiver surface. The increase in the evaporator temperature also increase the COP of the SEAS, while coefficient of performance decreases with rise in the generator temperature.

Nomenclature

k	Thermal conductivity [Wm^{-1} K]	$\dot{E}_{x,in}$	Exergy rate in [kW]
F_r	Heat removal factor	G_b	Solar radiation [Wm^{-2}]
h_{con}	Convection heat transfer [$Wm^{-2}K$]	h	Specific enthalpy [$kJ.kg^{-1}$]
$\dot{Q}_a$	Absorber heat [kW]	Q_u	Useful heat [kW]
U_L	Overall heat loss [$Wm^{-2}K$]	s	Entropy ($kJ.kg^{-1}K$)
φ	Nano particles %age	$\dot{\rho}_{nf}$	Density of nano fluid [kgm^{-3}]
μ	Dynamic viscosity [Pa s]	$\dot{\psi}_{dest}$	Exergy destruction rate [kW]
elec	Electrolyzer	HHV	High heating value of hydrogen
SEAS	Single effect absorption system		

References

[1] Loni, R. al., Thermodynamic analysis of a solar dish receiver using different nanofluids. Energy, 133 (2017), pp. 749-760.

[2] IRENA, Renewable power generation costs in 2012: an overview. Abu Dhabi: United Arab Emirates; 2012.

[3] Le Roux, WG. Et al., The efficiency of an open-cavity tubular solar receiver for a small-scale solar thermal Brayton cycle: Energy Convers Manag., 84 (2014), pp. 457-70.

[4] Qiu, K. et al., Simulation and experimental study of an air tube-cavity solar receiver: Energy Convers Manag., 103(2015), pp. 847-58.

[5] He, Y. et al., Experimental study on the light-heat conversion characteristics of nanofluids: Nanoscience and Nanotechnology Letters, 3(2011), pp. 494-96.

[6] Khullar, V. et al., Solar energy harvesting using nanofluids-based concentrating solar collector: Journal of Nanotechnology in Engineering and Medicine 3, 3 (2012): 031003
[7] Mahian, O. et al., Entropy generation during Al_2O_3/water nanofluid flow in a solar collector: effects of tube roughness, nanoparticle size, and different thermophysical models: Int J Heat Mass Transf, 78(2014), pp. 64-75.
[8] Sajid MU. and Ali HM., Recent advances in application of nanofluids in heat transfer devices: A critical review, Renewable and Sustainable Energy Reviews, 103 (2019), pp. 556-592.
[9] Pavlovic, S. et al., Thermal and exergetic investigation of a solar dish collector operating with mono and hybrid nanofluids: Thermal Science, 22 (2018), pp. 1383-1393.
[10] Ahmed, O. K. and Bawa, S. M., The combined effect of nanofluid and reflective mirrors on the performance of PV/thermal solar collector: Thermal Science, (2018): doi.org/10.2298/TSCI171203092A
[11] Laaraba. A., Numerical study of heat transfer in a flat plat thermal solar collector with partitions attached to its glazing: Thermal Science, (2018): doi.org/10.2298/TSCI170531101L
[12] Pavlovic, S. et al., Daily performance of a solar dish collector: Thermal Science, (2018): doi.org/10.2298/TSCI180124098P
[13] Montes, M. J. et al., Performance of a direct steam generation solar thermal power plant for electricity production as a function of the solar multiple: Solar Energy, 83(2009), pp. 679–689.
[14] Spelling, J., Favrat, D., Martin, A., and Augsburger, G., Thermoeconomic optimization of a combined-cycle solar tower power plant: Energy, Elsevier Ltd, 41(2012), pp. 113–120.
[15] Al-Sulaiman, F. A., Exergy analysis of parabolic trough solar collectors integrated with combined steam and organic Rankine cycles: Energy Conversion and Management, Elsevier Ltd, 77(2014), pp. 441–449.
[16] Dincer I, Rosen MA., Exergy, energy, environment and sustainable development: Oxford: Elsevier, 2007.
[17] Ahmadi, P et al., Exergo-environmental analysis of an integrated organic Rankine cycle for trigeneration: Energy Convers Manag., 64(2012), pp. 447-53.
[18] Caliskan, H. et al., Exergoeconomic and environmental impact analyses of a renewable energy based hydrogen production system: Int J Hydrogen Energy, 38(2013), pp. 6104-11.
[19] Parham, K. et al., Energy, exergy and environmental analysis of a novel combined system producing power, water and hydrogen: Energy, 134(2017), pp. 882-892.
[20] Abid, M. et al., Solar assisted multi-generation system using nanofluids: A comparative analysis: International Journal of Hydrogen Energy, 42(2017), pp. 21429 -21442.
[21] Ratlamwala, TAH. Et al., Performance analysis of a new designed PEM fuel cell: Int J Energy Res, 36(2012), pp.1121-32.
[22] Midilli, A. and Dincer, I., Development of some exergetic parameters for PEM fuel cells for measuring environmental impact and sustainability: Int J Hydrogen Energy, 34(2009), pp. 3858-72.
[23] Yilanci, A. et al., Performance analysis of a PEM fuel cell unit in a solar hydrogen system: Int J Hydrogen Energy, 33(2008), pp. 7538-52.
[24] Hollmuller, P. et al., Evaluation of a 5 kW photovoltaic hydrogen production and storage installation for a residential home in Switzerland: Int J Hydrogen Energy, 25(2000),pp. 97-109.
[25] Kalinci, Y. et al., Energy and exergy analyses of a hybrid hydrogen energy system: a case study for Bozcaada. Int J Hydrogen Energy, (2016), pp. 1-12.

[26] Ratlamwala, TAH. & Abid, M., Performance analysis of solar assisted multi-effect absorption cooling systems using nanofluids: A comparative analysis. International Journal of Energy Research, 42(2018), pp. 2901-15.
[27] Bahman, AMK., Modeling of solar-powered single-effect absorption cooling system and supermarket refrigeration/HVAC system, June 13, 2011.
[28] Asdrubali, F. et al., Solar cooling with small-size absorption chillers: different solutions for summer air conditioning." In Proceedings of the XIII European Conference IIR—Centro Studi Galileo, Milano, Italy, 2009. pp. 12-13
[29] De Vega, M. et al., Performance of a LiBr–water absorption chiller operating with plate heat exchangers: Energy conversion and management, 47, no. 18-19 (2006), pp. 3393-3407.
[30] Khanafer, K. & Vafai, K., A critical synthesis of thermophysical characteristics of nanofluids: Int. J. Heat. Mass Transf, 54(2011), pp. 4410-4428.
[31] Khan, M. S. et al., Energy, Exergy and Economic Feasibility Analyses of a 60 MW Conventional Steam Power Plant Integrated with Parabolic Trough Solar Collectors Using Nanofluids: Iranian Journal of Science and Technology, Transactions of Mechanical Engineering, (2018), 1-17.
[32] Colburn AP., A method for correlating forced convection heat transfer data and a comparison with fluid friction: Trans. Am. Inst Chem Engrs, 29(1933), pp. 174-210.
[33] Ngo, L. C., Exergetic Analysis and Optimization of a Parabolic Dish Collector for Low Power Application, Center for Renewable and Sustainable Energy Studies. University of Pretoria: (2013)
[34] Sheykhlou, H. & Jafarmadar, S., Analysis of a combined power and ejector–refrigeration cycle based on solar energy: Iranian Journal of Science and Technology, Transactions of Mechanical Engineering, 40(2016), pp. 57-67.
[35] Gebreslassie BH. Et al., Exergy analysis of multieffect water–LiBr absorption systems: from half to triple effect: Renew Energy, 35(2010), pp. 1773-1782.
[36] Ratlamwala, TAH. Et al., Exergetic and Environmental Impact Assessment of an Integrated System for Utilization of Excess Power from Thermal Power Plant. In Causes, Impacts and Solutions to Global Warming, Springer, New York, NY, 2013, pp. 803-824
[37] Gomri, R., Second law comparison of single effect and double effect vapour absorption refrigeration systems: Energy Conversion and Management, 50(2009), pp. 1279-1287.
[38] Cengel, YA., Boles, MA., Thermodynamics: an engineering approach. 7th ed. New York, McGraw-Hill; in SI units, 2017